

Conditional Moment Closure and G-equation Hybrid Modelling For Dual-Fuel Methane/N-Heptane Combustion

Bruno S. Soriano¹, Edward S. Richardson¹, Yuri M. Wright², Stephanie Schlatter²

¹ University of Southampton

² ETH Zurich

Abstract

Lean premixed combustion of natural gas in IC engines is attractive since it combines low emissions with diesel-like efficiencies due to the high knock resistance of natural gas. The low ignition propensity of natural gas however poses significant challenges in terms of robust combustion initiation with conventional spark plugs, especially at lean conditions. Dual-fuel combustion, where a more reactive diesel micro pilot is injected to provide a reliable source of ignition for the natural gas, constitutes a very promising alternative. Following ignition, flame propagates through a partially-reacted and inhomogeneous mixture of the two fuels. This study formulates and tests turbulent combustion modelling for dual-fuel engines using different models depending on the flame burning mode. The hybrid model combines Conditional Moment Closure (CMC) modelling, accounting for the autoignition of the n-heptane spray, with the G-equation model describing the subsequent flame propagation. The modelling is tested against previous measurements of dual-fuel methane/n-heptane combustion in a Rapid Compression Machine experiment. The new numerical methodology couples the models to account for the heat release from both fuels and can be used for the full range of fuel substitution, from pure diesel to pure natural gas engines. The results present a good agreement with experimental data with respect to cumulative heat release.

1. Introduction

Gas fuelled and pilot ignited dual fuel combustion has proven to be a promising concept for exploiting alternative fuels such as natural gas in internal combustion engines, potentially achieving lower CO₂ emissions and reducing major pollutants such as NO_x and PM [1,2]. The use of natural gas combines a high octane number, suitable for engines with efficient high compression ratios, with a high carbon-to-hydrogen ratio, both leading to a substantial reduction in carbon dioxide emissions.

The combustion initiation in dual fuel engines is fundamentally different compared to premixed systems ignited by a spark plug since an additional more reactive fuel is present and ignition is determined by the reaction kinetics and turbulence in the pilot spray. Pilot-ignited dual-fuel combustion involves a complex transition between the pilot fuel autoignition and a premixed-like phase of combustion, involving combinations of combustion processes – autoignition, diffusion flames, and flame propagation through inhomogeneous reactant mixtures – that present a challenge for predictive combustion modelling [3,4]. Hence premixed combustion models are suitable only for the treatment of the flame propagation phase in the gas/air mixture after ignition of the pilot spray.

A number of attempts on dual-fuel engine modelling have been reported in recent years involving mostly phenomenological (see for example [5–7]) and quasi-two zone [8] up to multi-zone [9] models. In the framework of multidimensional combustion simulation for pilot injected gas engines,

modelling efforts are sparse. In Refs. [10] and [11], dual fuel combustion was modelled by an adaptation of the characteristic timescale model (CTC), originally developed for diffusion-controlled combustion, and an extension of the model to account for addition of natural gas. Diesel and natural gas were lumped together to represent the fuel scalar in the combustion model according to their mass fractions in the respective cell of the computational domain and under the assumption that both the diesel and natural gas react at the same reaction rates. Ignition was then modelled using the Shell ignition model [12,13] which can successfully capture the auto-ignition of hydrocarbons in high-temperature and high-pressure environments. In this formulation the Shell model cannot account for the influence of the gaseous fuel on the ignition process of the pilot fuel, although, as presented in Ref. [6], the addition of methane has a substantial impact on the autoignition kinetics of diesel-like fuels. The model predictions for heat release rates, pressure evolutions and emissions were in good agreement with experimental results for natural gas substitution rates up to 90% (10% diesel fuel pilot quantity). However, with substitution contents above 90%, where pilot masses are small, the agreement deteriorated rapidly due to the CTC model's inability to accurately track flame propagation processes. In order to account for the premixed flame propagation process of dual fuel combustion, an extended model was proposed in Ref. [14]. A level-set approach (G-equation) was chosen for the modelling of the premixed turbulent flame,

* Corresponding author: b.soriano@soton.ac.uk
Proceedings of the European Combustion Meeting 2017

which was extended with a new formulation for the determination of the laminar flame speed by chemistry tabulation. Due to the application of multiple models to cater for different stages in the dual fuel combustion process, a careful implementation of the coupling between those models is needed [14]. The extension to the G-equation model for the premixed combustion phase resulted in close agreement with experimental heat release profiles for natural gas substitution rates up to 98%. Furthermore, it was highlighted that accurate laminar flame speed data for engine-like conditions is required to predict flame propagation rates and flame-wall interactions affecting emission of unburned hydrocarbons. A similar hybrid approach was presented by Cordiner et al. [15], combining the Shell ignition model with the coherent flame model where deviations from the experiment during ignition come from the heat released by pilot not being accounted in the simulation.

The objective of this study is to investigate the performance of a new approach for modelling pilot-ignited dual-fuel combustion systems, and to validate these developments by comparison with high-quality experimental measurements. N-heptane and methane are used as surrogates of diesel and natural gas, respectively. A state-of-art model for autoignition and diffusion flames, Conditional Moment Closure (CMC), is coupled with the level-set G-equation model to account for the flame propagation. The combustion models are coupled in such way, presented later, that the heat released comes from both fuels. The ignition delay time is determined by the turbulence-combustion interaction and the chemical scheme utilized which considers the gas fuel. The G-equation uses an advanced laminar flame speed model to account for mixture inhomogeneity and cool flame effects. Therefore, the new implementation should be able to capture the ignition delay time and heat released for the full range of fuel substitution.

2. Formulation

2.1 Flow field solver

The flow field is simulated using the Reynolds Averaged Navier Stokes (RANS) equations and a Lagrangian spray model implemented in the STAR-CD software [16]. The effects of gas-phase turbulence are modelled by the RNG variant of the $k-\varepsilon$ model [17]. Spray processes are modelled using sub-models offered within STAR-CD and described in Ref. [17], including: STAR-CD's standard drag, heat and mass transfer correlations; the Reitz atomization model; the Reitz-Diwakar secondary breakup model [18]; the Bai droplet interaction model; and the O'Rourke model for droplet-wall collisions. Droplet thermophysical properties (heat capacity, viscosity, latent heat, vapor pressure, density and surface tension) are modelled within STAR-CD as a function of temperature [17]. In order to account for cavitation effects, the nozzle contraction coefficient is adjusted to a value of 0.9 in order to give similar accuracy for pilot spray vapour penetration across all operating points, leading to a nominal orifice diameter of 122 μm .

Due to the off-centre location of the pilot single hole injector, a 180deg sector of the combustion chamber was modelled. The base resolution of the trimmed mesh is 1 mm, and the region surrounding the pilot nozzle and spray are refined with a characteristic cell dimension of 0.5mm, in order to ensure a ratio of cell size/nozzle diameter of 3.7, in accordance with good practice discussed in Refs.[19,20]. The computational grid consists of 270,000 cells at the start of the simulation and 105,000 cells at TDC. Mesh motion is performed with experimentally-derived piston position files for each operating point, and all initial conditions were set according to the average data obtained from thermodynamic analysis of the respective operating points [21] summarized in Table 1.

Table 1. Operating points selected for multidimensional combustion simulation.

Operation Point	OP2	OP3
ϕ_{CH_4}	0.44	0.60
T [K] at SOI	776	823
P [bar] at SOI	17.8	
Pilot injection [mg]	1.40	

2.2 G-equation model

The premixed phase is modelled using the level-set or G-equation approach to describe premixed flame propagation [22]. Ignition of the premixed flame by the pilot spray is modelled using a separate combustion model based on Conditional Moment Closure, described in Section 2.3. The scalar variable G is a distance function from the instantaneous flame position. The G-equation modelling for turbulent combustion employed in this study is based on the evolution of the modelled Favre mean and variance equations for G [23]:

$$\bar{\rho} \frac{\partial \tilde{G}}{\partial t} + \bar{\rho} \tilde{u} \cdot \nabla \tilde{G} = \bar{\rho} s_T |\nabla \tilde{G}| - \bar{\rho} \frac{\mu_T}{Sc_{\tilde{G}}} \tilde{\kappa} |\nabla \tilde{G}| \quad [1]$$

and

$$\begin{aligned} \bar{\rho} \frac{\partial \tilde{G}''^2}{\partial t} + \bar{\rho} \tilde{u}_j \cdot \nabla \tilde{G}''^2 &= \nabla_{\parallel} \cdot \left(\bar{\rho} \frac{\mu_T}{Sc_{\tilde{G}}} \nabla_{\parallel} \tilde{G}''^2 \right) + \\ 2\bar{\rho} \frac{\mu_T}{Sc_{\tilde{G}}} (\nabla \tilde{G})^2 - c_s \bar{\rho} \frac{\tilde{\varepsilon}}{\tilde{\kappa}} \tilde{G}''^2. \end{aligned} \quad [2]$$

s_T is the turbulent flame speed modelled as a function of the turbulence intensity u' and the laminar flame speed s_L modelled as

$$s_T = s_L \left[1 + A \left(\frac{u'}{s_L} \right)^{5/6} \right]. \quad [3]$$

Sc_G is the turbulent Schmidt number for the moments of the G-field, and μ_T is the turbulent viscosity given by the $k-\varepsilon$ model. All turbulent Schmidt numbers are set equal to 0.7. The velocity fluctuation u' is calculated from the turbulent kinetic energy $u' =$

$\left(\frac{2}{3}\tilde{k}\right)^{1/2}$. A mean progress variable \tilde{c}_G is mapped to the simulated G-moment fields according to

$$\tilde{c}_G = a_3 \left[\operatorname{erf} \left(\frac{a_1 \tilde{c}}{l_{F,T}} - a_2 \right) + 1 \right], \quad [4]$$

where $(a_1, a_2, a_3) = (1.8, 2.9, 0.5)$ [17] and $l_{F,T}$ is the turbulent flame brush thickness, which is calculated as

$$l_{F,T} = \alpha \frac{\sqrt{G'^T}}{|\nabla \tilde{c}|}. \quad [5]$$

where α is a model constant with the default value 1.0. The calculation of the mean species mass fractions using \tilde{c} is presented in the Section 2.5.

2.3 Conditional Moment Closure Ignition Model

Pilot spray ignition is modelled by a two-dimensional Conditional Moment Closure (CMC) model. This approach assumes that the methane mass fraction is uniform prior to injection of n-heptane. An advantage of the CMC approach is that it accommodates arbitrarily complex chemical kinetics, including both n-heptane and methane fuels, and accounts for composition variation associated with turbulent fluctuations of mixture fraction. In combination with a presumed-probability density function (PDF) for the mixture fraction distribution, the CMC model provides a prediction of the unconditional mean composition in each CFD cell. The CMC formulation and implementation adopted are based on the work of Wright et al. [24]. Essential details of the CMC implementation are presented here and the reader is referred to Ref. [25,26] for further information.

The CMC approach assumes that the thermochemical state in the turbulent flow can be represented adequately by conditional averages –in this study, conditional on the mixture fraction of n-heptane. The conditional average mass fraction Q_α of species α and the conditionally-averaged temperature Q_T are defined by,

$$Q_\alpha(\eta; x, t) = \langle Y_\alpha(x, t) | \xi(x, t) = \eta \rangle \quad [6]$$

and

$$Q_T(\eta; x, t) = \langle T(x, t) | \xi(x, t) = \eta \rangle \quad [7]$$

where η is the sample space variable for mixture fraction. Klimenko [1990] and Bilger [1993] developed conditionally-averaged transport equations for Q_α

$$\frac{\partial Q_\alpha}{\partial t} + \langle v | \eta \rangle \cdot \nabla Q_\alpha = \langle N | \eta \rangle \frac{\partial^2 Q_\alpha}{\partial \eta^2} + \langle \omega_\alpha | \eta \rangle - \frac{\nabla \cdot \left(\langle v'' Y_\alpha'' | \eta \rangle \tilde{P}(\eta) \right)}{\tilde{P}(\eta)}. \quad [8]$$

The corresponding transport equation for Q_T is

$$\begin{aligned} \frac{\partial Q_T}{\partial t} + \langle v | \eta \rangle \cdot \nabla Q_T &= \langle N | \eta \rangle \left[\frac{\partial^2 Q_T}{\partial \eta^2} + \right. \\ &\left. \frac{1}{\langle c_p | \eta \rangle} \left(\frac{\partial \langle c_p | \eta \rangle}{\partial \eta} + \sum_{\alpha=1}^N \langle c_{p,\alpha} | \eta \rangle \frac{\partial Q_\alpha}{\partial \eta} \right) \frac{\partial Q_T}{\partial \eta} \right] - \\ &\frac{1}{\langle c_p | \eta \rangle} \sum_{\alpha=1}^N \langle h_\alpha \omega_\alpha | \eta \rangle - \frac{\nabla \cdot \left(\tilde{P}(\eta) \langle v'' T'' | \eta \rangle \right)}{\tilde{P}(\eta)} + \frac{\partial p / \partial t}{\langle c_p | \eta \rangle \langle p | \eta \rangle}. \end{aligned} \quad [9]$$

2.4 Numerical implementation of CMC

The CMC equations are discretized with finite difference, using second order central differences for diffusive terms and first order upwind differencing for convective terms. Time integration is achieved using a stiff ODE solver and operator splitting, as described in Refs. [25,27,28].

Noting that conditional moments show weak spatial variation compared to unconditional moments, the spatial CMC grid is less refined than the CFD grid and, following several previous studies involving spray auto ignition [25,28–31], the conditional statistics are assumed to be homogeneous in the direction azimuthal to the injector axis. The cartesian CMC grid has two spatial dimensions, with 30 cells evenly spaced in the radial direction and 13 cells in the direction of the cylinder axis which change the size in accordance with the moving CFD grid [26]. The grid has 101 grid points in mixture fraction space clustered around the n-heptane/air stoichiometric value.

2.4.1 CMC sub-models

The CMC implementation in this paper uses a first order approximation to close the reaction source term, function of the conditionally averaged thermochemical state. The local rate of change of pressure, last term in the RHS of Eq. (9), is obtained from the CFD solution. The conditional turbulent fluxes of species mass fractions $\langle u_i'' Y_\alpha'' | \eta \rangle$ and temperature $\langle u_i'' T'' | \eta \rangle$ are closed assuming gradient transport and employing the unconditional turbulent diffusivity μ_T / Sc_ξ . The conditional velocity is closed using the linear model [32]. Local pressure fluctuations are neglected. The conditional scalar dissipation rate in each CFD cell, $\langle N | \eta \rangle_{CFD}$, is modelled using the amplitude mapping closure [33]

$$\langle N | \eta \rangle_{CFD} = N_0 G(\eta) \quad [10]$$

where $G(\eta)$ is a bell-shaped function with unity amplitude,

$$G(\eta) = \exp(-2[\operatorname{erf}^{-1}(2\eta - 1)]^2) \quad [11]$$

and the amplitude of the scalar dissipation rate profile is given by,

$$N_0 = \frac{\tilde{\chi}}{2 \int_0^1 G(\eta) \tilde{P}(\eta) d\eta}. \quad [12]$$

The Favre probability density function for the mixture fraction, $\tilde{P}(\eta)$, is modelled by a beta-function, using

the Favre mean and variance of mixture fraction in each CFD cell. The CFD and CMC grids are not necessarily the same, and a pdf-weighted averaging procedure is used to obtain the conditional scalar dissipation rate for each CMC cell,

$$\langle N | \eta \rangle = \frac{\sum (\bar{\rho} \bar{P}(\eta) \cdot \langle N | \eta \rangle_{CFD} \cdot V)}{\sum (\bar{\rho} \bar{P}(\eta) \cdot V)}, \quad [13]$$

where the summation is over all of the CFD cells contained within that CMC cell and V is the volume of the respective CFD cells.

2.4.2 Ignition chemistry

The 44-species skeletal n-heptane mechanism by Liu et al. [34] is used in the ignition model. The Liu et al. mechanism provides predictions in reasonable agreement with more detailed schemes concerning ignition delay times of n-heptane/methane blends. It is seen that the mechanism performs less well in relation to flame propagation through n-heptane/methane blends. However, the CMC model is only used for the ignition prediction, the flame speeds are based on empirical formulae presented in Section 2.2, rather than depending on the kinetic mechanism used for the CMC. The thermodynamic state is modelled using the ideal gas equation and temperature-dependent specific heats in accordance with Liu et al. [34].

2.5 Model coupling

The unconditional hydroxyl (OH) radical mass fraction computed only by the CMC is used to start the G-equation calculation. When it exceeds 4e-4, the cell is considered to have ignited, and a burnt condition is imposed in the G-equation solution for that cell. The predictions are found to be insensitive to the value chosen for the OH threshold, likely because thermal runaway occurs rapidly following the start of high-temperature ignition.

The G-equation model originally implemented in Star-CD uses the mean progress variable to compute a one-step reaction. In this new implementation, where G-equation is coupled with CMC, both share the same chemical scheme.

The unconditional mean composition in each CFD cell is computed by weighting the burnt and unburnt unconditional mean compositions considering the maximum value of the mean progress variable from each model, as presented in Eqs. (14-15). The CMC progress variable \tilde{c}_{CMC} is based on temperature, whereas the mean G-eq progress variable is defined in Eq. (4).

$$\tilde{c}_{max} = \max[\tilde{c}_{CMC}, \tilde{c}_G] \quad [14]$$

$$\tilde{Y}_i = (1 - \tilde{c}_{max}) \tilde{Y}_{i,u} + \tilde{c}_{max} \tilde{Y}_{i,b} \quad [15]$$

The unburnt $\tilde{Y}_{i,u}$, burnt $\tilde{Y}_{i,b}$ and \tilde{c}_{CMC} are obtained by integration the conditional quantities over the PDF, as presented in Eq. (16) for a generic scalar θ .

$$\tilde{\theta} = \int_0^1 \langle \theta | \eta \rangle \tilde{P}(\eta) d\eta \quad [16]$$

The conditional unburnt mixture remains constant over the simulation and corresponds to the initial condition. The conditional burnt composition is obtained from an equilibrium solver and updated every time step due to the pressure change caused by the piston motion and combustion. The temperature in the physical space is computed by Star-CD considering the enthalpy of the mixture and the composition given by Eq. (15).

3.Results

The results are presented in terms of cumulative heat release, defined as the integral of the heat release rate from the start of injection to each point in time. The heat release rate is computed as the difference between the internal energy computed by an isentropic compression and the actual internal energy affected by pressure rise. The same methodology was applied in both numerical and experimental data.

The experimental cases are very distinct regarding the combustion regimes involved. The OP2 corresponds to a lower initial temperature and lower flame speeds also due to the lean equivalence ratio. Figure 1 presents the experimental and numerical data for the OP2 test case with respect to cumulative heat release rate and time after the start of injection (SOI). The dash-dotted lines correspond to the amount of energy from the n-heptane mass injected (lower), and the energy contained in the methane/air mixture. A fast but small increase in cumulative heat release is observed, corresponding to the n-heptane autoignition. After the heat released reaches the n-heptane energy threshold, a steady increase is observed driven by flame propagation mainly after the TDC (vertical grey line in Fig. 1). The numerical scheme is not able to accurately capture the ignition delay time, a difference of 0.51ms or 62% was obtained. The difference arises from the fact that the chemical mechanism was not validated for dual-fuel conditions. The numerical result shows a faster burn rate compared to the measurement, with a difference of 30 J in the cumulative heat released at TDC. The CMC model, from where the burnt composition is taken in the coupling, is not accounting for heat transfer to the wall what may cause the over prediction of heat released. The causes of the difference in burn rate still needs further analysis also regarding the laminar flame speed. However, preliminary results have shown a weak dependence of heat release rate on laminar flame speed under similar conditions.

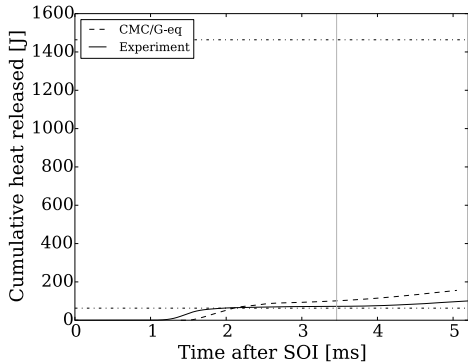


Fig. 1 – Cumulative heat release rate for the OP2 test case

Figure 2 shows the temperature contour plot for the OP2 test case at different times. The models coupling is clear in Fig. 2a, with a hot diffusion flame at the centre of a cooler lean premixed flame ignited by the n-heptane injection. Fig 2b shows a later stage where all n-heptane was burnt and the premixed flame remains. Figure 2b, in accordance with Fig. 1, also highlights the slow flame propagation (compared to Fig. 2a) and the small portion of the domain where combustion is happening.

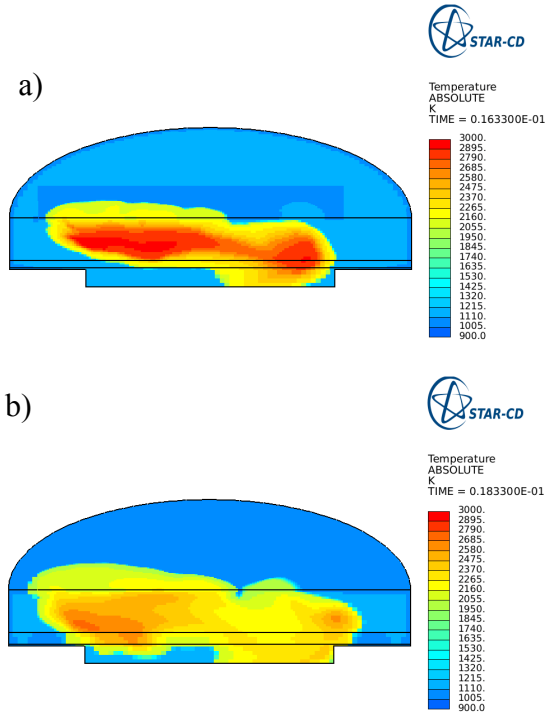


Fig. 2 – OP2 temperature contour plot at: a) 2.26ms; b) 4.65ms after SOI.

In the OP3 test case, the higher temperature and equivalence ratio make possible a faster flame propagation after ignition and consequent increase of heat released presented in Fig. 3. The numerical scheme presented a better agreement in terms of ignition delay time. A difference of 0.26ms or 22% was found. A sharp increase in heat released after 4 ms corresponds to the autoignition of the premixed charge. This condition where different combustion modes are present at the same time, also seen in HCCI

engines, is a challenge for all combustion models available. However, the solution from the CMC was able to capture the trend. The earlier autoignition is can be attributed to the n-heptane chemical mechanism, that is predicting the autoignition of a pure methane/air mixture.

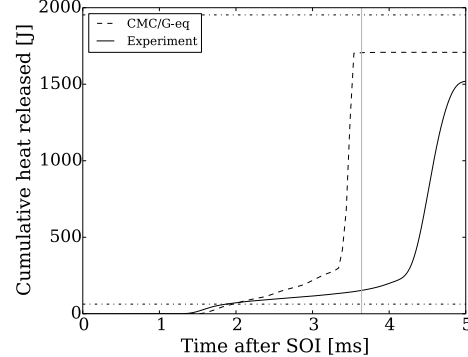


Fig. 3 – Cumulative heat release rate for the OP3 test case

In order to show that the sharp rise on heat released is coming from an autoignition, Figure 4 presents the temperature contours for the instant where the maximum gradient of cumulative heat release occurs. Apart from the already ignited region, all domain is experiencing the same temperature rise from the methane autoignition. Unburnt temperatures around 1300K are seen prior the methane reaction. The model is not able to capture gradients of methane ignition delay time close to the wall due to different unburnt temperatures as may be seen in the experiment.

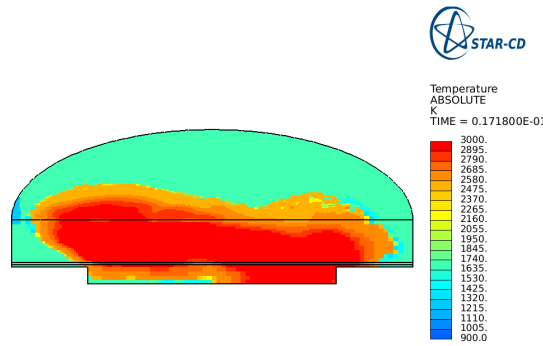


Fig. 4 – OP3 temperature contour plot at 3.39ms after SOI.

4. Conclusion

The paper presented a numerical and experimental study of dual-fuel combustion in a RCEM machine. A new hybrid numerical scheme was developed where the autoigniting diffusion flame is computed using the CMC and the premixed phase is captured by G-equation. The model was successfully implemented in a commercial software capable of solving real engine cases.

The modelling was able to capture with good accuracy the transition between the diffusion and premixed flames in the OP2 case. The solution of the conditional space is not accounting for heat transfer to

the wall, and can be one of the sources for the greater heat released.

The results for the OP3 test case have shown the modelling capability to capture different combustion modes, starting from the autoignition of a diffusion flame and ignition of the premixed charge, the premixed flame propagation and finally the autoignition of all mixture.

Further analyses of laminar flame speed model, heat transfer to the walls in the CMC energy equation and chemical schemes are necessary in order to improve the modelling accuracy.

5. Acknowledgements

The authors are thankful for financial support from CNPq (Brazil) grant number 207250/2014-6.

6. References

- [1] R.. Papagiannakis, D.. Hountalas, Experimental investigation concerning the effect of natural gas percentage on performance and emissions of a DI dual fuel diesel engine, *Appl. Therm. Eng.* 23 (2003) 353–365. doi:10.1016/S1359-4311(02)00187-4.
- [2] G.H. Abd Alla, H.A. Soliman, O.A. Badr, M.F. Abd Rabbo, Effect of pilot fuel quantity on the performance of a dual fuel engine, *Energy Convers. Manag.* 41 (2000) 559–572. doi:10.1016/S0196-8904(99)00124-7.
- [3] Z. Wang, J. Abraham, Fundamental physics of flame development in an autoigniting dual fuel mixture, *Proc. Combust. Inst.* 35 (2015) 1041–1048. doi:10.1016/j.proci.2014.06.079.
- [4] E. Demosthenous, G. Borghesi, E. Mastorakos, R.S. Cant, Direct Numerical Simulations of premixed methane flame initiation by pilot n-heptane spray autoignition, *Combust. Flame.* 163 (2016) 122–137. doi:10.1016/j.combustflame.2015.09.013.
- [5] M. Mbarawa, B.E. Milton, R.T. Casey, Experiments and modelling of natural gas combustion ignited by a pilot diesel fuel spray, *Int. J. Therm. Sci.* 40 (2001) 927–936. doi:10.1016/S1290-0729(01)01279-0.
- [6] M. Mbarawa, B.E. Milton, R.T. Casey, H. Miao, Fuel injection characteristics of diesel-stimulated natural gas combustion, *Int. J. Energy Res.* 23 (1999) 1359–1371. doi:10.1002/(SICI)1099-114X(199912)23:15<1359::AID-ER560>3.0.CO;2-7.
- [7] C. Mansour, A. Bounif, A. Aris, F. Gaillard, Gas–Diesel (dual-fuel) modeling in diesel engine environment, *Int. J. Therm. Sci.* 40 (2001) 409–424. doi:10.1016/S1290-0729(01)01223-6.
- [8] G.H. Abd Alla, H.A. Soliman, O.A. Badr, M.F. Abd Rabbo, Combustion quasi-two zone predictive model for dual fuel engines, *Energy Convers. Manag.* 42 (2001) 1477–1498. doi:10.1016/S0196-8904(00)00143-6.
- [9] J.B. Liu, G.A. Karim, Simulation of combustion processes in gas-fuelled diesel engines, *Proc Instn Mech Engrs.* 211 (1997) A.
- [10] Y. Zhang, S. Kong, R.D. Reitz, Modeling and Simulation of a Dual Fuel (Diesel / Natural Gas) Engine With Multidimensional CFD, *SAE Tech. Pap.* 2003-01-0755. (2003) 1–14.
- [11] S. Singh, S. Kong, R. Reitz, S. Krishnan, K. Midkiff, Modeling and experiments of dual-fuel engine combustion and emissions, (2004). <http://papers.sae.org/2004-01-0092/>.
- [12] M.P. Halstead, L.J. Kirsch, C.P. Quinn, The autoignition of hydrocarbon fuels at high temperatures and pressures—Fitting of a mathematical model, *Combust. Flame.* 30 (1977) 45–60. doi:10.1016/0010-2180(77)90050-5.
- [13] K. SC, R. RD, Multidimensional Modeling of Diesel Ignition and Combustion Using a Multistep Kinetics Model, *ASME. J. Eng. Gas Turbines Power.* 115 (1993) 781–789. doi:10.1115/1.2906775.
- [14] S. Singh, L. Liang, S.-C. Kong, R.D. Reitz, Development of a Flame Propagation Model for Dual-Fuel Partially Premixed Compression Ignition Engines, *Int. J. Engine Res.* 7 (2006) 65–75. doi:10.1243/146808705X7464.
- [15] S. Cordiner, V. Rocco, R. Scarcelli, M. Gambino, Experiments and Multi-Dimensional Simulation of Dual-Fuel Diesel/Natural Gas Engines, *SAE Tech. Pap.* (2007) 18. doi:10.4271/2007-24-0124.
- [16] CD-adapco, CD-adapco website, (n.d.). <http://www.cd-adapco.com/> (accessed August 1, 2015).
- [17] CD-adapco, Star cd ® version 4.24 Methodology, (2015).
- [18] R. Reitz, R. Diwakar, Effect of Drop Breakup on Fuel Sprays, *SAE Tech. Pap.* (1986). doi:10.4271/860469.
- [19] G. Pizza, Y.M. Wright, G. Weisser, K. Boulouchos, Evaporating and non-evaporating diesel spray simulation : comparison between the ETAB and wave breakup model, *Int. J. Veh. Des.* 45 (2007) 80–99. doi:10.1504/IJVD.2007.013672.
- [20] Sandia National Laboratory, Engine Combustion Network, (2014). <http://www.sandia.gov/ecn/>.
- [21] S. Schlatter, Experimental and Numerical Characterization of Enhanced Ignition Systems for Large Bore Gas Engines, ETH-Zürich, 2015. doi:10.3929/ethz-a-010410665.
- [22] F.A. Williams, The Mathematics of Combustion, in: J.D. Buckmaster (Ed.), Society for Industrial & Applied Mathematics, 1985: pp. 197–1318.
- [23] N. Peters, Turbulent combustion, Cambridge University Press, Cambridge, 2004.
- [24] Y. WRIGHT, G. DEPAOLA, K. BOULOUCHOS, E. MASTORAKOS, Simulations of spray autoignition and flame establishment with two-dimensional CMC, *Combust. Flame.* 143 (2005) 402–419. doi:10.1016/j.combustflame.2005.08.022.
- [25] Y.M. Wright, Numerical investigation of turbulent spray combustion with Conditional Moment Closure, (2005). doi:10.3929/ethz-a-005228336.
- [26] G. de Paola, Conditional Moment Closure for Autoignition in Turbulent flows, Univ. Cambridge, (2007).
- [27] G. de Paola, E. Mastorakos, Y.M. Wright, K. Boulouchos, Diesel Engine Simulations with Multi-Dimensional Conditional Moment Closure, *Combust. Sci. Technol.* 180 (2008) 883–899. doi:10.1080/00102200801894273.
- [28] Y.M. Wright, O.N. Margari, K. Boulouchos, G. De Paola, E. Mastorakos, Experiments and simulations of n-heptane spray auto-ignition in a closed combustion chamber at diesel engine conditions, *Flow, Turbul. Combust.* 84 (2010) 49–78. doi:10.1007/s10494-009-9224-0.
- [29] M. Bolla, D. Farrace, Y.M. Wright, K. Boulouchos, E. Mastorakos, Influence of turbulence–chemistry interaction for n-heptane spray combustion under diesel engine conditions with emphasis on soot formation and oxidation, *Combust. Theory Model.* 18 (2014) 330–360. doi:10.1080/13647830.2014.898795.
- [30] M. Bolla, T. Gudmundsson, Y.M. Wright, K. Boulouchos, Simulations of Diesel Sprays Using the Conditional Moment Closure Model, *SAE Int. J. Engines.* 6 (2013) 1249–1261. doi:10.4271/2013-01-1618.
- [31] G. Borghesi, E. Mastorakos, C.B. Devaud, R.W. Bilger, Modeling evaporation effects in conditional moment closure for spray autoignition, *Combust. Theory Model.* 15 (2011) 725–752. doi:10.1080/13647830.2011.560282.
- [32] A.Y. Klimenko, R.W. Bilger, Conditional moment closure for turbulent combustion, *Prog. Energy Combust. Sci.* 25 (1999) 595–687. doi:10.1016/S0360-1285(99)00006-4.
- [33] E.E. O'Brien, T.-L. Jiang, The conditional dissipation rate of an initially binary scalar in homogeneous turbulence, *Phys. Fluids A Fluid Dyn.* 3 (1991) 3121. doi:10.1063/1.858127.
- [34] S. Liu, J.C. Hewson, J.H. Chen, H. Pitsch, Effects of strain rate on high-pressure nonpremixed n-heptane autoignition in counterflow, *Combust. Flame.* 137 (2004) 320–339. doi:10.1016/j.combustflame.2004.01.011.